Scientia Iranica C (2022) 29(6), 3208–3217

Sharif University of Technology
Scientia Iranica
Transactions C: Chemistry and Chemical Engineering
http://scientiairanica.sharif.edu

A hybrid model for simulation of lithium-ion batteries using artificial neural networks and computational fluid dynamics

F. Dehghani[a], R. Eslamloueyan[a,*], and M. Sarshar[b,*]

a. *School of Chemical and Petroleum Engineering, Shiraz University, Molasadra Ave., Shiraz, Iran.*
b. *Institute of Mechanics, Iranian Space Research Center, Falasiri Street, Shiraz, Iran.*

Received 25 October 2021; received in revised form 14 February 2022; accepted 9 May 2022

KEYWORDS
Artificial neural networks;
Lithium-ion batteries;
Electrochemical and thermal simulation;
Thermal management;
CFD simulation.

Abstract. Chemical reactions inside lithium-ion batteries generate heat and cause temperature rise. Hence, it is necessary to monitor battery time-dependent heat generation. In this work, a hybrid model for simulating heat generation inside a pack of lithium batteries was developed. An Artificial Neural Network (ANN) was employed to simulate electrochemical and thermal behaviors of a Panasonic NCR 18650 lithium-ion battery. In order to develop the hybrid model, the designed ANN was inserted into ANSYS Fluent software through a C source code. A 3D Computation Fluid Dynamics (CFD) was developed to simulate temperature distribution in the battery pack. Experimental data were obtained using a NEWARE battery test system at different C-rates. The outputs of the proposed ANN consist of heat generation inside the battery as well as the electrochemical parameters. The combination of the ANN and CFD modeling, which led to a hybrid model, can be mentioned as the major contribution of this work. The results exhibit excellent consistency between the proposed model and test data. The simulation estimates the range of the manufacturer's working temperatures (-20 to 60°C) regarding the considered batteries.

1. Introduction

Increase in fossil fuel consumption worldwide has been responsible for global warming, a result of greenhouse effect due to excessive CO_2 production. It is predicted that with the current rate of fuel consumption, global petroleum reserves will be exhausted in the next 50 years [1]. According to these facts, the need for renewable and sustainable energy sources is becoming more evident than ever before. Energy sources contain batteries, fuel cells, capacitors, etc.

Batteries can be used as both primary and backup energy sources in the electrical devices like Electric Vehicles (EVs), Hybrid Electric Vehicles (HEVs), communication systems, and so on [2]. Nowadays, lithium-ion batteries are the leading batteries with special characteristics that include fast response, high energy density, high nominal voltage, low self-discharge rate, long cycle life, and no memory effect [3–5].

In spite of these positive characteristics, performance and safety of lithium-ion batteries must be monitored during operation to avoid sudden expul-

*. *Corresponding authors. Tel./Fax: +98 711 6231388*
E-mail addresses: eslamlo@shirazu.ac.ir (R. Eslamloueyan); m.sarshar@isrc.ac.ir (M. Sarshar)

doi: 10.24200/sci.2022.59292.6160

sion [6]. Even the best performing systems are prone to degradation over time and usage. For example, three important accidents that led to high economic damage to companies that use lithium-ion batteries as their source of energy are as follows:

1. In September 2016 a Samsung Galaxy Note 7 battery malfunctioned causing about $3 billion in losses [7];
2. Plane crash in April 2000 caused by failure of the power supply system of its landing gear;
3. Accident of Mars Global Surveyor in November 2006 due to heating of battery radiators [8,9].

It is concluded from the past accidents and problems caused by malfunctioning of lithium-ion batteries that monitoring and predicting battery heat generation and its working temperature are crucial for battery performance.

There is no simple and accurate model available to predict lithium-ion battery characteristics such as cycle life, capacity, heat generation, etc. Developing tools that provide information such as voltage, remaining capacity, heat generation, and other battery operational characteristics at every desired time and working cycle is necessary. To achieve this goal, the Artificial Neural Networks (ANNs) as one of the most powerful black box modeling techniques with quick responses is used to predict electrochemical and thermal characteristics of lithium-ion batteries.

ANNs are useful for non-linear systems and those that cannot be described by analytical equations. ANNs are considered as data-based models that are able to learn from experiments and examples [10].

ANNs have been used to predict electrochemical properties of lithium-ion batteries such as voltage, capacity, power, and other battery parameters such as State of Charge (SoC), State of Health (SoH), and State of Energy (SoE) [10–17]. Parthiban et al. employed artificial neural network for the first time to predict the electrochemical characteristics of lithium-ion batteries [10].

Several cooling methods are used for temperature control inside battery pack based on the amount of heat generated during battery operation and the environmental conditions, taking into account the best operating temperatures in the range of 20 to 40°C [18]. Cooling methods are applied by gas and liquid [19] using phase-change materials [10] and heat pipes [20].

Computational fluid dynamics is an effective way to simulate temperature distribution inside battery pack. Wang et al. developed a Computation Fluid Dynamics (CFD) simulation to find the temperature distribution inside a single cylindrical lithium-ion battery cell, considering that no cooling strategy is applied in order to control the temperature distribution [21].

Cicconi et al. studied temperature distribution in an electric vehicle battery pack, calculated heat generation inside battery for different C-rates, and finally considered three forced convection cooling methods for thermal management of battery pack [22].

The novelty of this work is the combination of an ANN black box model with a CFD model for developing a hybrid model to simulate a pack of commercial Li-ion batteries. After constructing the neural network, it is integrated with Fluent software through a C code in order to simulate the temperature distribution inside the battery pack.

2. Methodology

The acquired experimental data and thermal model adopted in this study, constructing structure of the network along with the pattern employed to optimize the number of hidden layer neurons, and the battery pack structure are discussed in this section.

2.1. Data acquisition

In order to obtain experimental data such as voltage, temperature, capacity, etc., a host computer, NEWARE BTS 3000 battery test system, and an incubator are used. The battery test system is shown in Figure 1. Data acquisition system and the way all components interact with each other are shown in Figure 2. All training and testing data are collected from NCR 18650 Panasonic lithium-ion cell. Data obtained include cycle number, time, and voltage at constant temperatures of 25, 35, and 45°C for 0.5, 1.0, and 1.5 C-rate for discharge. Time steps for data gathering are one second for total times of 6700 s, 3700 s, and 1300 s for discharge rates of 0.5 C, 1.0 C, and 1.5 C, respectively. The overall data for battery simulation is shown in Table 1.

Figure 1. BTS3000 Neware Battery Tester for obtaining experimental data.

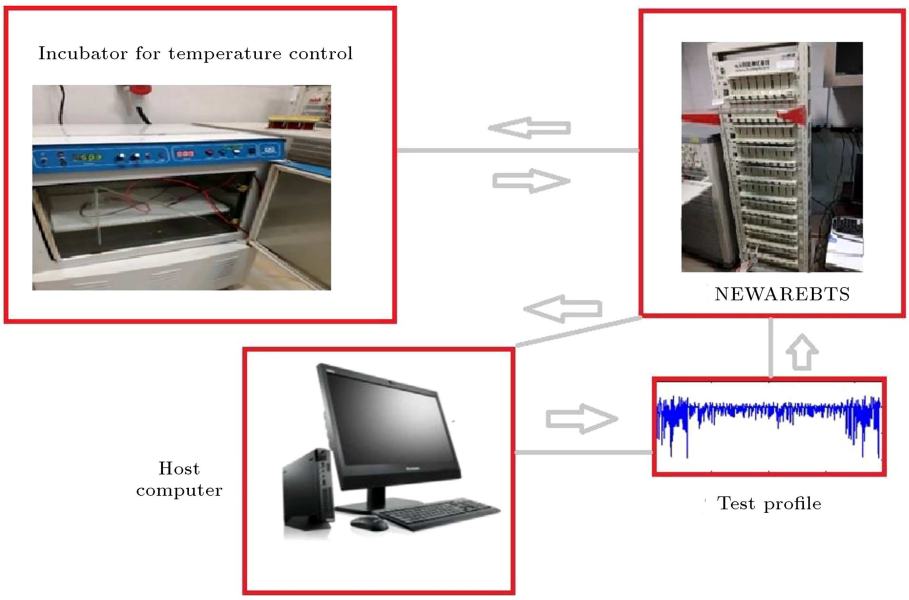

Figure 2. Battery data acquisition system.

Table 1. Overall battery cell data.

Discharge rate	0.5 C	1.0 C	1.5 C
Cycles	30	30	30
Cell voltage	2.58–4.00	2.65–3.85	2.68–3.78
Time (s)	6700	3700	1300
Cell temperature (K)	298–318	298–318	298–318

2.2. Thermal model

The most common equation that is used for calculating heat generation inside a battery during an electrochemical process is shown in Eq. (1) [23]:

$$Q = I(V_0 - V) - IT\frac{dV_0}{dT}. \quad (1)$$

Q is heat generation in the battery, V_0 Open-Circuit Voltage (OCV), V cell voltage, I applied current (positive for discharging and negative for charging), and T temperature of the cell. The first term in Eq. (1) is the overpotential due to ohmic losses in the cell, charge transfer overpotentials at the interface, and mass transfer limitations. The second term is the entropic heat, and the potential derivative with respect to temperature is considered as the entropic heat coefficient [24].

2.3. Measurement of entropy change

The following method is used to measure the entropic heat generation of the battery [25]:

1. Keeping cell at OCV for about 21–23 h at room temperature;
2. Temperature change by 10°C after every 2.5 h;
3. V_0 measurement at temperatures 25, 35, 45, and 55°C.

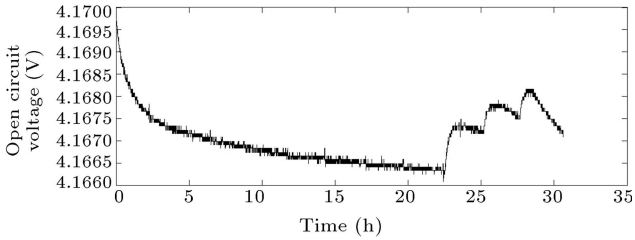

Figure 3. OCV versus time for calculation of entropic heat coefficient.

As is shown in Figure 3, OCV decreases while the battery is kept at 25°C for about 22 hours due to self-discharge [26]. When the temperature is changed from 25°C to 35°C, OCV increases in a short period of time, then it decreases again as time goes on. The same procedure is applied at 45°C and 55°C. $\frac{dV_0}{dT}$ is calculated for each increase in OCV using least squares approximation assuming that the changes in OCV trend are linear.

2.4. Artificial neural network

Artificial neural network is a black box model that links input to output data using a defined set of nonlinear functions. ANNs are inspired by biological nervous systems [27] and the basic unit in ANN is the neuron [28]. They are trained using a number of input data with corresponding output data obtained from actual measurements so that a particular set of inputs produces a specific set of target outputs. Training network adjusts weights and biases in such a way that outputs match the targets as much as possible. It is important to construct the best architecture of ANN by choosing appropriate training algorithm and transfer functions.

As input and output data are determined, de-

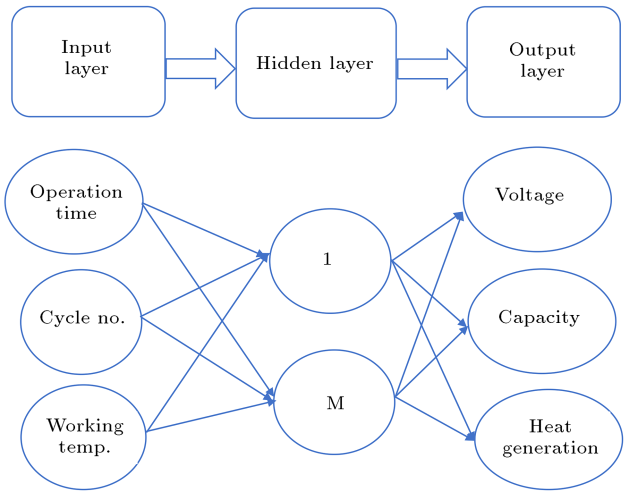

Figure 4. Input/output of the neural network.

signing ANN architecture is initiated. In this study, a feedforward multilayer perceptron of MATLABs neural network toolbox is used. ANN training is more efficient through proper normalization of the data. Normalization of inputs is performed using Eq. (2) in the range of −1 to 1.

$$x = \frac{2(x - x_{\min})}{x_{\max} - x_{\min}} - 1, \tag{2}$$

where $x_{\min}$ and $x_{\max}$ are the minimum and maximum of the input vector of x in the neural network, respectively. Tansigmoide is the type of neurons transfer function being used which is shown in Eq. (3):

$$f(x) = \frac{\exp(x) - \exp(-x)}{\exp(x) + \exp(x)}. \tag{3}$$

In this work, feed-forward network is used. The Levenberg-Marquardt backpropagation algorithm [29–31] is used to minimize the Mean Squared Errors (MSE) between the experimental and calculated outputs by adjusting the weights and biases. ANNs are prone to data overfitting; therefore, the dataset is divided into three subsets: training, validation, and testing [32]. For each case, 70% of the dataset is selected for training, 15% for validation, and 15% for random testing. Randomization is performed before training.

2.4.1. Input and output of neural network

Operation time, cycle number, and working temperature are the inputs, while heat generation (Q), voltage, and capacity are the output of the network. The input/output of the neural network is shown in Figure 4.

2.5. Selection of optimal configuration

Several methods are proposed in the literature for approximating the number of hidden layer neurons in ANNs. One of the proposed methods, named pyramid rule, is used for a three-layered neural network. In this method, the number of hidden layer neurons is estimated by $\sqrt{(a * b)}$, in which a and b represent the number of input and output layer neurons [33]. Katz implies that the number of hidden layer neurons can be from one half to three times the number of input neurons [34]. In this work, a cross-validation method is employed to optimize the number of hidden layer neurons [35]. Cross-validation method is a usual method in machine learning in order to prevent data over-fitting. It is based on training the network with a small number of neurons; and if the test data error does not meet the goal, the number of hidden layer neurons is increased by one. This procedure is repeated until increase in the number of hidden layer neurons causes test error growth. Errors are reported as Mean Relative Error (MRE) and MSE shown in Eqs. (4) and (5), respectively:

$$MRE = \frac{1}{N}\sum_{i=1}^{N}\frac{|x_{\exp} - x_{\text{pred}}|}{x_{\exp}}, \tag{4}$$

$$MSE = \frac{1}{N}\sum_{i=1}^{N}(x_{\exp} - x_{\text{pred}})^2. \tag{5}$$

N is the number of data points; $x_{\exp}$ and x_{pred} are the experimental and predicted values of the outputs.

2.6. Battery pack design

Battery pack consists of 24 commercially available NCR 18650 Panasonic lithium-ion batteries in a 3×8 array configuration. There is 2 mm space between batteries (for each row and column) and 5 mm space from the pack body. Each battery is 18.5 mm in diameter and 65.5 mm height with nominal voltage of 3.6 V and capacity of 2900 mAh.

Some cooling methods are used for controlling battery pack temperature. All sides of battery pack are isolated except bottom of the pack which is connected to a heat sink. In addition, cooling via natural convection with two sides of the battery pack exposed to atmosphere is examined.

2.7. Battery pack thermal model

Thermal modeling of the battery pack is carried out using CFD simulation. Data from thermal modeling of a single cell battery based on artificial neural networks are used for thermal modeling of the battery pack. A C code for the insertion of single cell thermal model into the CFD simulation software is developed. The flow chart of the whole simulation is shown in Figure 5.

2.7.1. CFD methodology and boundary conditions

In case where the battery pack is cooled via natural convection, laminar flow is used as the fluid flow and the energy equation is activated. Least squared cell-based equations as the gradient equations, second-

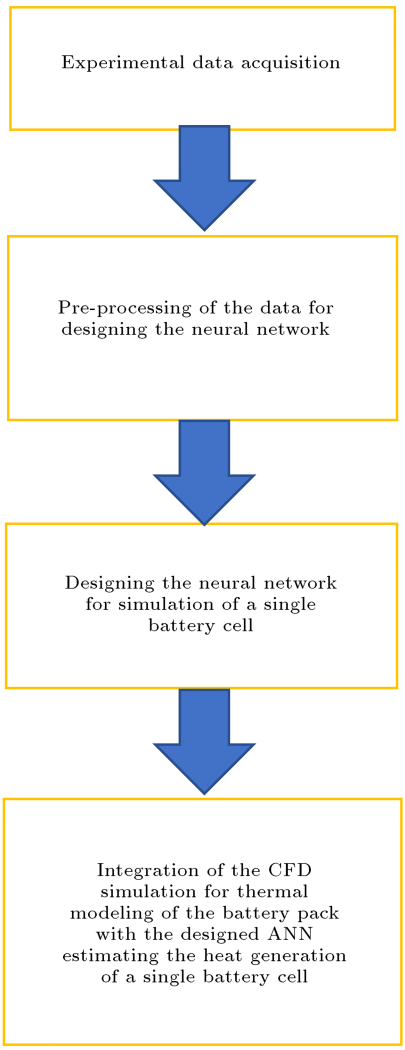

Figure 5. The flow chart of the whole simulation.

order equations as the pressure model, and second-order upwind equations as the momentum and energy equations are activated. In another case, only energy equation is activated where cooling is carried out through a heat sink, steady state simulation, and pressure-based solver, which are the other governing conditions used in the simulation.

2.7.2. Creating the geometry

GAMBIT 2.2 is used in order to both create the geometry and produce optimized mesh. GAMBIT provides different options for meshing such as hexahedral, hexahedral wedge, and tetrahedral hybrid mesh. In this study, hexagonal mesh is chosen because of the simplicity of the geometry. The major superiorities of GAMBIT over other geometry and mesh creating tools are optimizing and creating the best mesh near boundaries, thus ensuring higher accuracy. In order to select the best mesh, the process begins with the small number of nodes and then, the aspect ratio and mesh quality are checked. This process is repeated for different node numbers; finally, the optimized values of 25 cell zones, 137483 faces, and 738249 nodes are obtained.

3. Results and discussion

3.1. Neural networks

The results of cross-validation method applied to the network for optimizing hidden layer neurons are shown in Figures 6 to 8. A range of errors based on different neurons and C-rates are shown in Tables 2 to 4. In these tables, MSE and MRE are reported for test data based on the calculated errors and optimized number of hidden layer neurons for C-rate of 0.5, 1.0, and 1.5.

Optimized number of hidden layer neurons is listed in Table 5. MSE for training, validation, and test data shows the high level of accuracy of the network for

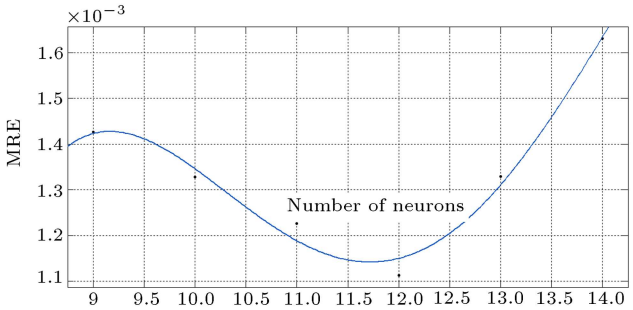

Figure 6. Number of hidden layer neurons versus MRE for 0.5 C discharge.

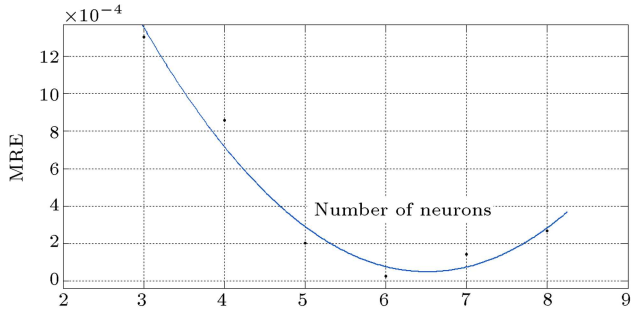

Figure 7. Number of hidden layer neurons versus MRE for 1 C discharge.

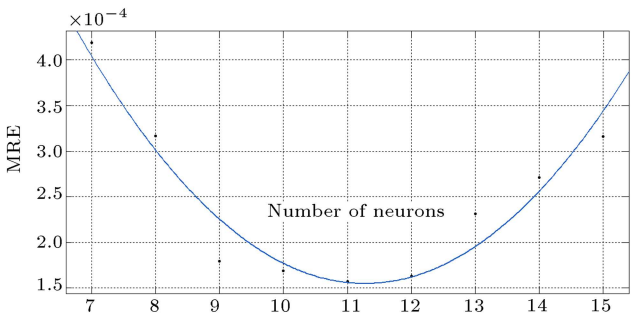

Figure 8. Number of hidden layer neurons versus MRE for 1.5 C discharge.

Table 2. MRE and MSE for different neural network configurations for 0.5 C discharge.

Number of neurons	MRE	MSE
9	1.10×10^{-3}	1.42×10^{-3}
10	1.03×10^{-3}	1.69×10^{-3}
11	1.07×10^{-3}	1.48×10^{-3}
12	1.07×10^{-3}	1.11×10^{-3}
13	1.32×10^{-3}	1.32×10^{-3}
14	1.06×10^{-3}	1.63×10^{-3}

Table 3. MRE and MSE for different neural network configurations for 1.0 C discharge.

Number of neurons	MRE	MSE
3	1.30×10^{-3}	3.09×10^{-3}
4	8.57×10^{-4}	4.28×10^{-4}
5	2.03×10^{-4}	3.15×10^{-4}
6	2.64×10^{-5}	2.74×10^{-4}
7	1.43×10^{-4}	2.50×10^{-4}
8	7.80×10^{-4}	1.31×10^{-4}

Table 4. MRE and MSE for different neural network configurations for 1.5 C discharge.

Number of neurons	MRE	MSE
10	1.69×10^{-4}	1.08×10^{-4}
11	1.57×10^{-4}	6.06×10^{-5}
12	1.63×10^{-4}	2.54×10^{-5}
13	2.31×10^{-4}	6.71×10^{-5}
14	2.71×10^{-4}	6.76×10^{-5}
15	3.16×10^{-4}	8.03×10^{-5}

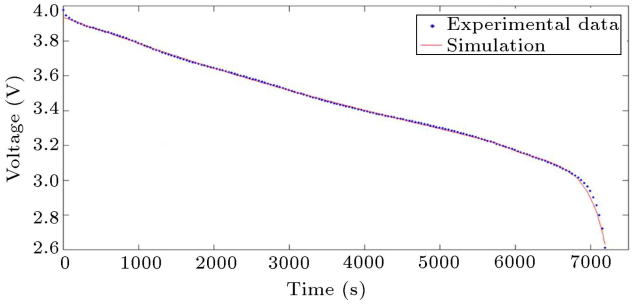

Figure 9. Voltage versus time for 0.5 C discharge test data.

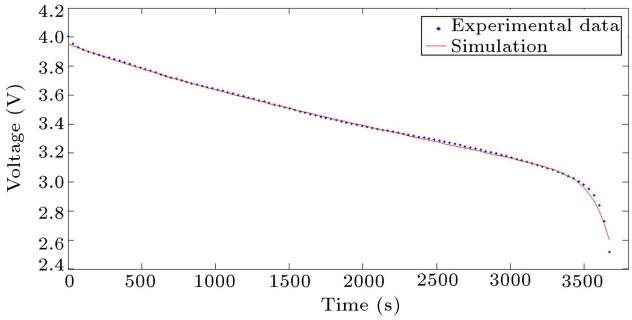

Figure 10. Voltage versus time for 1 C discharge test data.

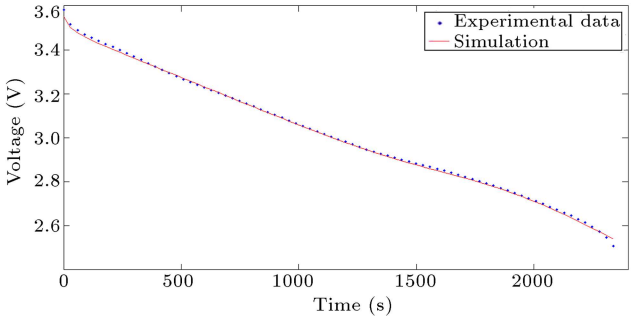

Figure 11. Voltage versus time for 1.5 C discharge test data.

prediction. MRE is used for test data (which is already used for optimizing hidden layer neurons) with error percentage of less than 0.1 for all cases.

Voltage versus time for 0.5, 1.0, and 1.5 C in discharge are shown in Figures 9 to 11. It is understood that by increasing the C-rate, discharge time decreases. At the end of discharge, there is a steep decrease in voltage. This decrease is due to concentration polarization that happens due to lithium-ion concentration gradient in the battery. The smooth decrease of voltage in the middle of discharge also occurs because of ohmic polarization that happens due to non-ideality of electrodes and connections in the battery structure.

The capacity versus time in discharge for prediction and experimental data for C-rates equal to 0.5, 1.0, and 1.5 are shown in Figures 10 to 12. The capacity

Table 5. Number of hidden layer neurons, training, validation, and test data errors.

Discharge rate	No. of hidden layer neurons	Training data performance (MSE)	Validation data performance (MSE)	Test data performance (MSE)	Test data performance (MRE)
0.5 C	12	1.1×10^{-3}	1.1×10^{-3}	1.1×10^{-3}	10^{-3}
1.0 C	6	2.5×10^{-4}	3.3×10^{-4}	2.7×10^{-4}	2.6×10^{-5}
1.5 C	11	6.2×10^{-5}	5.9×10^{-5}	6.6×10^{-5}	1.5×10^{-4}

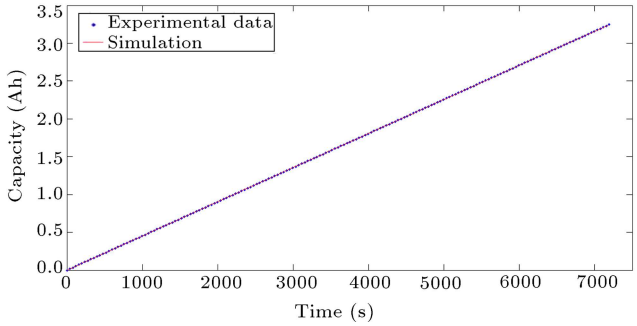

Figure 12. Capacity versus time for 0.5 C discharge test data.

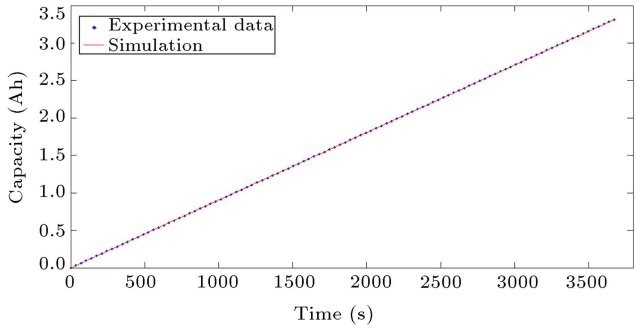

Figure 13. Capacity versus time for 1 C discharge test data.

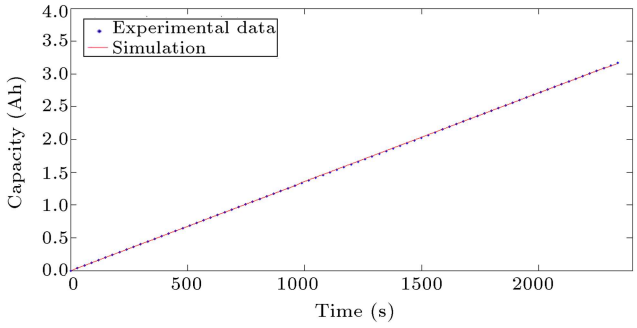

Figure 14. Capacity versus time for 1.5 C discharge test data.

has a linear behavior related to time and current and prediction curves exactly overlap the experimental data points.

Heat generation increases with time and the temperature is also increasing; therefore, temperature rise cannot solely affect the battery heat generation, as shown in Figures 13–15. Cell voltage in the first part of Eq. (1) plays an important role in the heat generation inside battery; therefore, the increase in the temperature merely decreases the intensity of heat generated. The heat generation versus time in discharge for C-rates equal to 0.5, 1.0, and 1.5 are shown in Figures 15 to 17. It can be seen that with increase in C-rate, heat generation increases and discharge time decreases.

3.2. CFD results

As C-rate increases, maximum temperature inside the

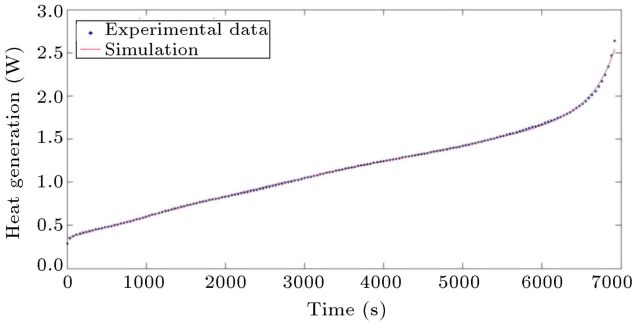

Figure 15. Heat generation versus time for 0.5 C discharge test data.

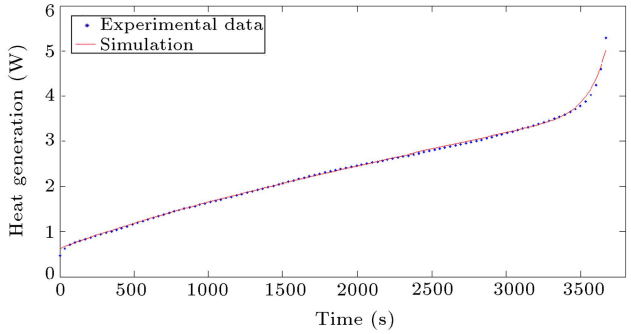

Figure 16. Heat generation versus time for 1 C discharge test data.

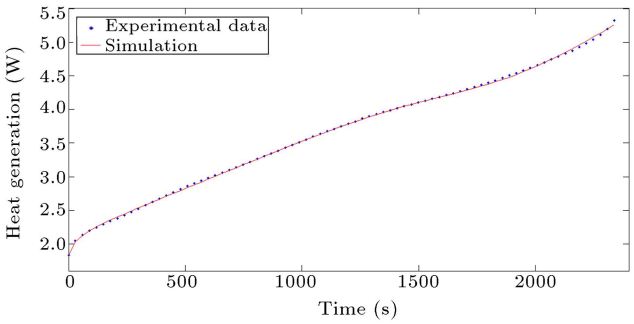

Figure 17. Heat generation versus time for 1.5 C discharge test data.

battery pack is increased, as shown in Figures 18 to 20. It is concluded from Bernardi equation that current and heat generations have a direct relation with each other. Higher C-rates are applied when higher levels of energies are demanded and stronger cooling systems are required. When cooling is carried out by natural convection and 0.5 C discharge rate, temperature of the battery pack is between 300–312 K on the outer sides and 310–324 K in the middle. At a discharge rate of 1.0 C, the temperature of the battery pack is between 311–330 K on the outer sides and 320–346 K in the middle. At a discharge rate of 1.5 C, the temperature of the battery pack is between 320–340 K on the outer sides and 340–362 K in the middle. When cooling is carried out by a heat sink in the vacuum condition and 0.5 C discharge rate, the temperature of the battery

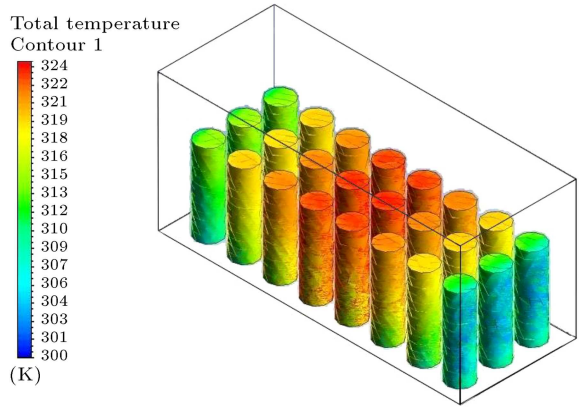

Figure 18. Battery pack under natural convection for 0.5 C discharge.

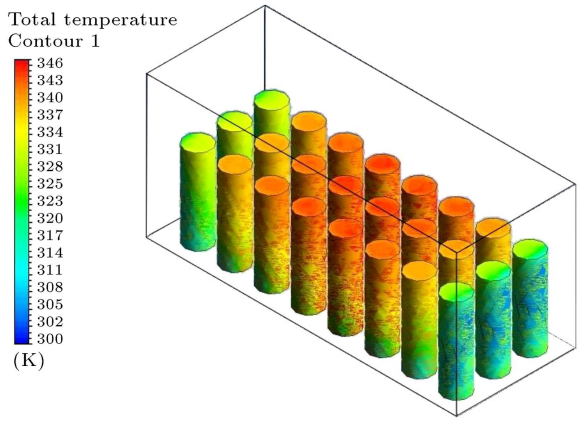

Figure 19. Battery pack under natural convection for 1 C discharge.

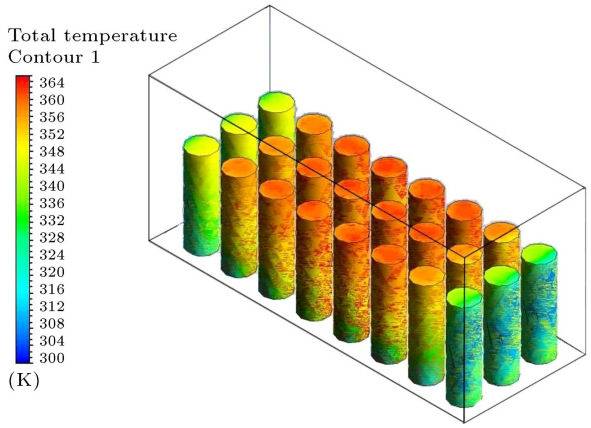

Figure 20. Battery pack with natural convection for 1.5 C discharge.

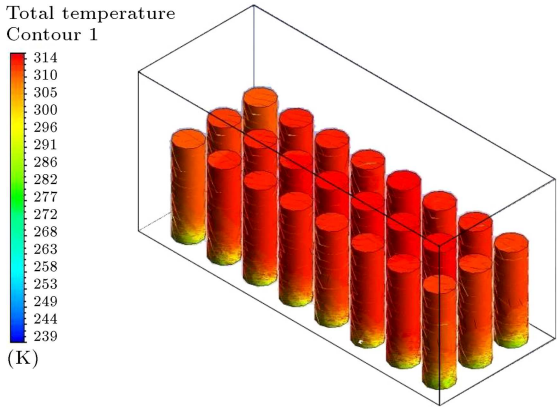

Figure 21. Battery pack under vacuum condition for 0.5 C discharge.

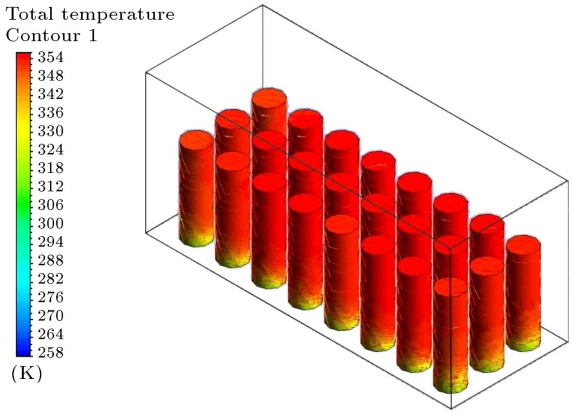

Figure 22. Battery pack under vacuum condition for 1 C discharge.

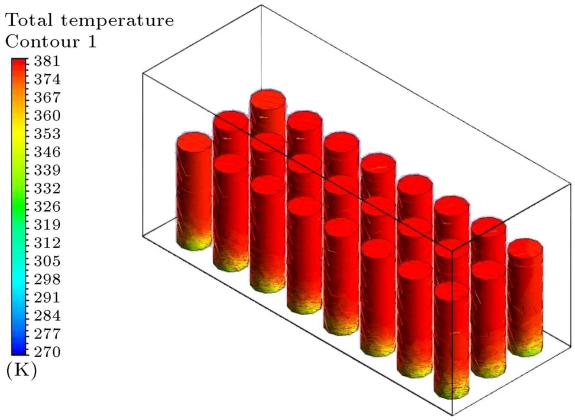

Figure 23. Battery pack under vacuum condition for 1.5 C discharge.

pack is between 286–305 K on the outer sides and 290–314 K in the middle. At a discharge rate of 1.0 C, the temperature of the battery pack is between 324–348 K on the outer sides and 330–354 K in the middle. At a discharge rate of 1.5 C, the temperature of the battery pack is between 332–381 K on the outer sides and 350–381 K in the middle. The simulation results under vacuum conditions are shown in Figures 21–23.

Maximum battery temperature occurs in the middle of the pack. This mainly happens because the lowest temperature difference is observed between cells and the circulated air around it. When pack walls and both ends are approached, temperature decreases in order to have a consistent temperature distribution over battery pack.

At equal C-rates, batteries in vacuum conditions

experience a higher temperature and pose a uniform temperature profile compared to natural cooling. This happens because conduction is the only way to extract heat from the battery pack in the vacuum, which has weak heat transfer compared to convection.

Optimal lithium-ion battery performance occurs at temperatures of 273 to 313 K, validating the CFD simulation in most cases. It can be seen that at higher C rates, the temperature inside the battery pack violates the optimum working temperature, but it is not significant because the batteries work at lower C-rates in most satellites.

4. Conclusion

Artificial neural networks were employed in order to simulate and predict the electrochemical and thermal properties of NCR 18650 lithium-ion batteries based on the experimental data points at 0.5, 1.0, and 1.5 C-rate discharge with 100 s time steps. Experimental data used to construct the network were divided into three classes: 70 percent of data for training, 15 percent for validation, and 15 percent for testing. Cross-validation method produces 12, 6, and 11 hidden layer neurons with mean relative errors of 10^{-3}, 2.6×10^{-5}, and 1.5×10^{-4} for test data for 0.5, 1.0, and 1.5 C-rates, respectively, indicating the quality and exactness of the simulation. After construction of the network, a C code, which contains network parameters, was incorporated into ANSYS Fluent software as a unique effort in this work. Computation Fluid Dynamics (CFD) simulation was performed for two separate cases of battery in the earth conditions with both ends of the battery pack being open and battery in the vacuum the same as space condition. The simulation of the hybrid model determined temperatures included in the range of the manufacturer's optimal working temperature of the considered lithium-ion batteries (-20 to 60°C).

For future work and to ensure enhancement of the project, experimental data can be gathered for a battery pack and comparison can be made between the current simulation and experimental data.

Acknowledgments

The technical and financial support provided by Institute of Mechanics is deeply appreciated.

References

1. Lahidji, R., Michalski, W., and Stevens, B. "The long term future for energy", In *Energy: The Next Fifty Years*, OECD Ed., 1st Edn., Paris, pp. 7–28 (1999).
2. Stroe, D., Swierczy, M., Stan, A., et al. "Accelerated lifetime testing methodology for lifetime estimation of lithium-ion batteries used in augmented wind power plants", *IEEE Trans. Ind. Appl.*, **50**(6), pp. 4006–4017 (2014).
3. Ling, Z., Wang, F., Fang, X., et al. "A hybrid thermal management system for lithium ion batteries combining phase change materials with forced-air cooling", *Appl. Energy*, **148**(C), pp. 403–409 (2015).
4. Ritchie, A. and Howard, W. "Recent developments and likely advances in lithium-ion batteries", *J. Power. Sources*, **162**(2), pp. 809–812 (2006).
5. Ye, Y., Saw, L.H., Shi, Y., et al. "Numerical analyses on optimizing a heat pipe thermal management system for lithium-ion batteries during fast charging", *Appl. Therm. Energy*, **86**(C), pp. 281–291 (2015).
6. Xing, Y., Miao, Q., Tsui, K.L., et al. "Prognostics and health monitoring for lithium-ion battery", *IEEE Int. Conf. on Intel. and Secu. Informatics*, Beijing, China, pp. 242–247 (2011).
7. Lawson, S., *The Note7 will Cost Samsung Another US$3 Billion in Profit*, PC Worlds News (2016). https://www.pcworld.idg.com.au/article/608533/note7-will-cost-samsung-another-3-billion-profit/
8. Goebel, K., Saha, B., Saxena, A., et al. "Prognostics in battery health management", *IEEE Instrum. Meas. Mag.*, **11**(4), pp. 33–40 (2008).
9. He, W., Williard, N., Osterman, M., et al. "Prognostics of lithium-ion batteries based on Dempster-Shafer theory and the Bayesian Monte Carlo method", *J. Power Sources*, **196**(23), pp. 10314–10321 (2011).
10. Parthiban, Th., Ravi, R., and Kalaiselvi, N. "Exploration of artificial neural network [ANN] to predict the electrochemical characteristics of lithium-ion cells", *Electr. Acta*, **53**(4), pp. 1877–1882 (2007).
11. Sbarufatti, C., Corbetta, M., Giglio, M., et al. "Adaptive prognosis of lithium-ion batteries based on the combination of particle filters and radial basis function neural networks", *J. Power Sources*, **344**, pp. 128–140 (2017).
12. He, W., Williard, N., Chen, Ch., et al."State of charge estimation for Li-ion batteries using neural network modeling and unscented Kalman filter-based error cancellation", *Int. J. Elec. Power and Energy. Syst.*, **62**, pp. 783–791 (2014).
13. Wang, L.K., Zhao, X., and Ma, J. "A new neural network model for the state-of-charge estimation in the battery degradation process", *Appl. Energy.*, **121**(C), pp. 20–27 (2014).
14. Chaoui, H., Ibe-Ekeoch, Ch.C., and Gualous, H. "Aging prediction and state of charge estimation of a LiFePO4 battery using input time-delayed neural networks", *Elec. Power Syst. Res.*, **146**, pp. 189–197 (2017).
15. Guo, Y., Zhao, Z., and Huang, L. "SOC estimation of lithium battery based on improved BP neural network", *Energy Procedia*, **105**, pp. 4153–4158 (2017).
16. Yang, D., Wang, Y., Pan, R., et al. "A neural network based state-of-health estimation of lithium-ion battery

in electric vehicles", *Energy Procedia*, **105**, pp. 2059–2064 (2017).

17. Dong, G., Zhang, Xu., Zhang, Ch., et al. "A method for state of energy estimation of lithium-ion batteries based on neural network model", *Energy*, **90**(p1), pp. 879–888 (2015).
18. Chang, W.Y. "Estimation of the state of charge for a LFP battery using a hybrid method that combines a RBF neural network, an OLS algorithm and AGA", *Int. J. Elec. Power and Energy Syst.*, **53**, pp. 603–611 (2013).
19. Somasundaram, K., Birgersson, E., and Mujumdar, A.S. "Thermal-electrochemical model for passive thermal management of a spiral-wound lithium-ion battery", *J. Power Sources*, **203**, pp. 84–96 (2012).
20. Sbarufatti, C., Corbetta, M., Giglio, M., et al. "Adaptive prognosis of lithium-ion batteries based on the combination of particle filters and radial basis function neural networks", *J. Power Sources*, **344**, pp. 128–140 (2017).
21. Wang, Zh., Ma, J., and Zhang, L. "Finite element thermal model and simulation for a cylindrical Li-Ion battery", *IEEE Access*, **5**, pp. 15372–15379 (2017).
22. Cicconi, P., Landi, D., and Germani, M. "Thermal analysis and simulation of a Li-ion battery pack for a lightweight commercial EV", *Applied Energy*, **192**(C), pp. 159–177 (2017).
23. Bernardi, D., Pawlikowski, E., and Newman, J. "A general energy balance for battery systems", *J. Electr. Society*, **132**(1), pp. 5–12 (1985).
24. Karimi, G. and Li, X. "Thermal management of lithium-ion batteries for electric vehicles", *Int. J. Energy Res.*, **37**(1), pp. 13–24 (2013).
25. Abdul-Quadir, Y., Laurila, T., Karppinen, J., et al. "Heat generation in high power prismatic Li-ion battery cell with $LiMnNiCoO_2$ cathode material", *Int. J. Energy Res.*, **38**(11), pp. 1424–1437 (2014).
26. Bandhauer, T.M., Garimella, S., and Fuller, T.F. "A critical review of thermal issues in lithium-ion batteries", *J. Elect. Society*, **158**(3), pp. R1–R25 (2011).
27. Wasserman, P.D. "Fundamentals of artificial neural networks", In *Neural Computing Theory and Practice*, Van Nostrant Reinhold Ed., 1st Edn., New York, pp. 11–27 (1989).
28. Beale, R. and Jackson, T. "The basic neoron", In *Neural Computing: An Introduction*, Teylor and Francis Croup LLC, 1st Edn., New York, pp. 39–57 (1990).
29. Levenberg, K. "A method for the solution of certain problems in least squares", *SIAM J. Numer. Anal.*, **16**, pp. 588–604 (1944).
30. Marquardt, D. "An algorithm for least-squares estimation of nonlinear parameters", *SIAM J. Appl. Math.*, **11**, pp. 431–441 (1963).
31. Hagan, M.T. and Menhaj, M. "Training feedforward networks with the Marquardt algorithm", *IEEE Trans. Neural Netw.*, **5**(6), pp. 989–993 (1994).
32. Hagan, M.T., Demuth, H.B., Beale, M.H., et al., *Neural Network Design*, Martin Hagan Ed., 2nd Edn., Singapore, pp. 37–43 (2014).
33. Masters, T., *Advanced Algorithms for Neural Networks: a C^{++} Sourcebook*, John Wiley & Sons, 1st Edn., UK (1995).
34. Katz, J.O. "Developing neural network forecasters for trading", *Tech. Anal. Stocks Commod.*, **10**(4), pp. 160–168 (1992).
35. Prechelt, L. "Automatic early stopping using cross validation: quantifying the criteria", *Neural Networks*, **11**, pp. 761–767 (1998).

Biographies

Farshad Dehghani is a process engineer at Hampa Energy Engineering and Design Company (HEDCO). He received the BS and MS degrees in Chemical Engineering from Shiraz University (Shiraz-Iran) in 2016 and 2018, respectively. His research interests include process simulation, fluid dynamics, and energy storage.

Reza Eslamnloueyan is a Professor in Chemical Engineering at Shiraz University. He received the BS and PhD degrees in Chemical Engineering from Sharif University of Technology (Tehran-Iran) in 1992 and 2003, respectively. He also earned his MS of Chemical Engineering from Shiraz University (Shiraz-Iran) in 1995. He joined the Department of Chemical Engineering at Shiraz University in 2004. His research interests include process modeling, simulation, design, and control in chemical engineering. Backed by twenty years of professional experience in process industries, he along with his colleagues established a knowledge-based company, Green Energy Science and Technology Company (GEST Co. ltd.), at Fars Science and Technology Park (FSTP) in 2011.

Mohammad Sarshar is an Associate Professor in Chemical Engineering at Iranian Space Research Center. He received the BS degree in Chemical Engineering from Sistan and Baluchistan University (Zahedan-Iran) in 1991. He also earned his MS and PhD of Chemical Engineering from Shiraz University (Shiraz-Iran) in 1995 and 2008, respectively. His research interests include process simulation, fuel, biofuel, and energy storage. Backed by thirty years of professional experience in technology development and process industries, he along with his colleagues established a knowledge-based company, Green Energy Science and Technology Company (GEST Co. ltd.), at Fars Science and Technology Park (FSTP) in 2011.